

Indirect frequency measurement of cable-stayed bridges in cross winds

J.D. YAU

Department of Architecture
Tamkang University
No.151, Yingzhuan Rd., Tamsui Dist., New Taipei City 25137
TAIWAN
jdyau@mail.tku.edu.tw

W.F. CHEN

Department of Civil Engineering,
National Taiwan University, Taipei City 106,
TAIWAN

S. URUSHADZE

Institute of Theoretical and Applied Mechanics
Academy of Sciences of the Czech Republic, v.v.i, Prague
CZECH REPUBLIC

Abstract: - In conventional bridge health monitoring, a number of sensors are deployed on a bridge directly for detecting its various dynamic properties. This is so called “direct method”. But the drawbacks of the direct method are: laborious deployment of sensors, time-consuming, and not portable. Following the previous Yang’s works (2004) in indirect method by using a passing test vehicle as a message receiver of bridge response, this study regards cross winds as lateral excitational sources to detect the lateral bridge frequencies from the lateral response of the moving test vehicle. To account for the wind-vehicle-bridge interactions in performing dynamic analysis, an iteration-based 3D vehicle-bridge interaction (VBI) finite element method is developed. The whole wind/VBI system is decomposed into two subsystems: the wind-bridge subsystem and the wind-vehicle subsystem. Then the iterative scheme is carried out to compute the interaction response between the two subsystems independently and iterate for removing unbalance forces. The numerical results indicated that the present indirect bridge monitoring is a simple and feasible method to measure the lateral frequency of a long-span bridge in cross winds.

Key-Words: - aerodynamics; frequency, indirect measurement, vehicle-bridge system; wind engineering

1 Introduction

In conventional bridge health monitoring, a number of vibration sensors should be deployed on the bridge directly. In general, the deployment and maintenance of a fixed sensor system is rather expensive, laborious, time-consuming, and lack of mobility. To circumvent the drawbacks of the fixed sensor system, an instrumented test vehicle was first proposed by Yang et al. (2004) for measuring the dynamic properties of a bridge. The so-called vehicle-bridge interaction (VBI) makes use of the interaction between the moving vehicle and the bridge. Such an approach has been referred to as the *moving-sensor system*, since the vehicle serving as a message carrier can virtually touch the entire span of the bridge and thus collect all the spatial information of the bridge. This approach has been

referred to as the *indirect approach* for measuring the bridge frequencies. Following this, Yang and co-workers (Lin and Yang 2005; Yang and Lin 2005; Yang and Chang 2009; Chang et al. 2011; Yang et al. 2012; Yang et al. 2013a-c; Yang et al. 2014) presented a series of experimental and theoretical investigations on the indirect measurement method. However, once the dynamic properties of a long-span bridge, such as cable-supported bridges, need to be measured, and comparative few works were investigated using the indirect measurement approach.

Due to the nonlinear and motion-dependent nature of wind loadings, the aerodynamic analysis of wind-induced response for cable supported bridges involves a tremendous amount of computations. Focusing on running safety of a train and the riding

comfort of passengers, Xu *et al.* (2003, 2004) adopted a 3D finite element model to investigate the aerodynamic response of suspension bridges and cable-stayed bridges carrying a train or road cars running over bridge deck in high winds. Cai and Chen (2004) presented a framework of dynamic analysis of coupled 3D vehicle-bridge system under strong winds to investigate the effects of driving speeds on dynamic performance of the vehicles as well as the bridge. Their results indicated that driving speeds of moving vehicles mainly affect the vehicle's vertical relative response while have insignificant effect on the rolling response of vehicles.

With the iteration-based computational techniques for wind/VBI system developed by Yau *et al.* (2014), this study tends to introduce the indirect measurement approach proposed by Yang *et al.* (2004) into the 3D finite element model for detecting the lateral bridge frequency of the vehicle-bridge system in cross winds. The wind loads acting on the bridge deck and car body are generated in time domain by digital simulation techniques that can account for the spatial correlation of stochastic wind velocity field. With motion-dependent nature of aerodynamic forces, a finite element modelling of the Kao-Pin-His (KPH) cable-stayed bridge will be employed to study the aerodynamic response of wind-vehicle-bridge interaction system. Then the dynamic response of the test vehicle moving on the bridge will be employed to extract the dynamic information of the bridge. From the present study, the first lateral bridge frequency can be detected, from which the proposed indirect bridge measurement method is feasible to monitor the lateral dynamic information of a long-span bridge in cross wind.

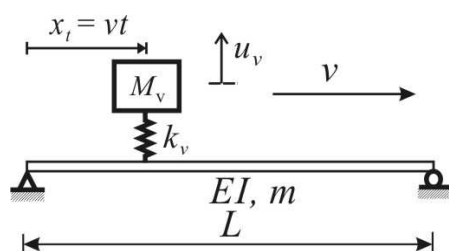


Fig. 1 Schematic of an un-damped VBI system.

2 Concept of indirect bridge monitoring

The equations of motion for the beam and the moving sprung mass with speed v are given by (Yang *et al.* 2004):

$$m\ddot{u} + EIu'''' = -(p_0 - M_v\ddot{u}_v)\delta(x - vt) \quad (1)$$

$$M_v\ddot{u}_v + k_v u_v = k_v u(x_t, t)$$

where $(\bullet)' = \partial(\bullet)/\partial x$, $(\bullet)\dot{=} \partial(\bullet)/\partial t$, $u(x, t)$ = vertical deflection of the beam, u_v = vertical displacement of the sprung mass, $p_0 = M_v g$ = weight of the sprung mass, g = acceleration of gravity, $\delta(\bullet)$ = Dirac's delta function, $H(t)$ = unit step function, and $x_t = vt$ = the position of the sprung mass on the beam. For a simply supported beam, the following boundary conditions are adopted:

$$u(0, t) = u(L, t) = 0, \quad EIu''(0, t) = EIu''(L, t) = 0 \quad (2)$$

The semi-complete solution of the vehicle's response for the sprung mass can be obtained as (Yang *et al.* 2004):

$$u_v(t) \approx \frac{\Delta_{s1}}{(1 - S_v^2)} \left[\frac{1}{2} \left(1 - \cos \frac{2\pi vt}{L} \right) - S_v^2 \sin^2 \frac{\omega_v t}{2} \right] + \frac{\Delta_{s1} S_1}{2} \times \left[C_{b1} \cos \left(\omega_b t - \frac{\pi vt}{L} \right) + C_{b2} \cos \left(\omega_b t + \frac{\pi vt}{L} \right) + C_v \cos(\omega_v t) \right] \quad (3)$$

where

$$S_1 = \pi v / \omega_b L, \quad S_v = 2\pi v / \omega_v L,$$

$$C_{b1} = \frac{-1}{1 - \left(\frac{\omega_b}{\omega_v} - \frac{S_v}{2} \right)^2}, \quad C_{b2} = \frac{1}{1 - \left(\frac{\omega_b}{\omega_v} + \frac{S_v}{2} \right)^2} \quad (4a-d)$$

and $C_v = -C_{b2} - C_{b1}$. As shown in Eqs. (3) and (4), the frequency ω_b of the beam has been captured in the vehicle's response. With this concept, the dynamic properties of the beam can be detected from the vehicle's response.

3 Simulation of wind loads

Wind-induced lateral vibration of cable-stayed bridges under the action of traffic flow is of concerns in this study. In this section, the wind loads acting on the vehicle-bridge system will be presented. The aerodynamic coefficient curves for the lift force and moment on the deck section are related to the angle of attack (Simiu and Scanlan 1996). The wind loads acting on the vehicle-bridge system are generated in the time domain by digital simulation techniques that can account for the spatial correlation of stochastic wind velocity field. Then an incremental iteration-based computational framework will be presented for dynamic analysis of the wind/VBI system.

3.1 Simulation of wind forces on bridge deck

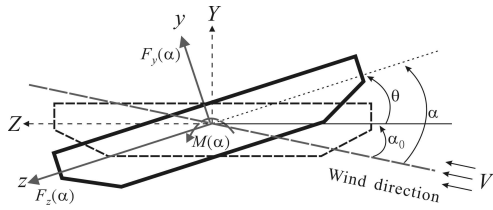


Fig. 2 Wind loads acting on the bridge section.

Figure 2 shows lateral wind load acting on the bridge deck with a mean velocity V and incident angle α_0 . As indicated, the effective angle α of attack along the oncoming wind flow can be expressed as $\alpha(x,t) = \alpha_0 + \theta(x,t)$. Since only the vertical and torsional vibrations of the beam are concerned, the lateral vibration of the beam caused by the aerodynamic drag force will be ignored. The aerodynamic lift force and pitching moment acting on the bridge deck can be expressed in terms of α as follows:

$$F_y(\alpha) = \frac{\rho V^2 B}{2} C_y(\alpha), F_z(\alpha) = \frac{\rho V^2 D}{2} C_z(\alpha), \quad (5a-d)$$

$$M(\alpha) = \frac{\rho V^2 B^2}{2} C_M(\alpha), \quad V = V_0 + v$$

where V_0 = velocity of mean wind, v_w = velocity of fluctuating wind, ρ = the air density, B = bridge deck width, D = bridge deck depth, C_z = aerodynamic lift coefficient, C_y = aerodynamic lateral coefficient, and C_M = aerodynamic moment coefficient.

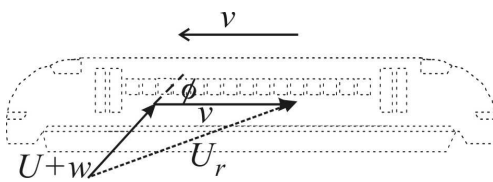


Fig. 3 Relative wind velocity and natural wind velocity to a moving vehicle

3.2 Simulation of quasi-steady aerodynamic forces on moving vehicle

Figure 3 shows the wind load model acting on a running vehicle with a mean velocity U and turbulent velocity w . The aerodynamic forces and moments acting at the mass centre of the moving vehicle are expressed as (Baker 1991):

$$F_S = \frac{\rho A_S U_r^2}{2} C_{cS}(\phi), M_Y = \frac{\rho A_S d_e U_r^2}{2} C_{cY}(\phi)$$

$$F_L = \frac{\rho A_T U_r^2}{2} C_{cL}(\phi), M_P = \frac{\rho A_T h_v U_r^2}{2} C_{cM}(\phi) \quad (7a-g)$$

$$U_r = \sqrt{[v + U \cos \phi]^2 + [(U + w) \sin \phi]^2}$$

$$\tan \phi = \frac{(U + w) \sin \phi}{v + U \cos \phi}$$

where ρ is the air density ($= 1.2\text{kg/m}^3$); A_S is the side surface area of the vehicle; A_T is the top surface area of the vehicle; d_e is the reference eccentricity of aerodynamic yawing moment about the mass centre; h_v is the reference height of vehicle's mass center; C_{cS} is aerodynamic coefficient of vehicle's side; C_{cL} is aerodynamic lift coefficient; C_{cP} is aerodynamic rolling moment coefficient; $\phi (= \arctan(U/v))$ is yaw angle (see Fig. 2); U_r is the relative wind velocity around the vehicle moving at speed v ; and w represent the turbulent wind speed component will be defined in the following section.

3.3 Simulation of turbulent wind velocity

To perform the interaction analysis of a maglev vehicle traveling over guideway under oncoming wind flows in the time domain, the following simplified spectral representation of turbulent wind (Xu et al. 2003) is employed to generate the time history of turbulent airflow velocity $w_j(t)$ in mean wind flow direction (lateral) at the j th point on the suspended beam as:

$$w_j(t) = \sqrt{2(\Delta\omega)} \sum_{n=1}^j \left[\sum_{i=1}^{N_f} \sqrt{S_w(\omega_{ni})} G_{jn}(\omega_{ni}) \cos(\omega_{ni}t + \psi_{ni}) \right] \quad (8)$$

where $j=1,2,\dots,N_s$, N_f is the total number of frequency intervals represented by a sufficiently large number; N_s is the total number of points along the guideway to simulate; $S_w(\omega)$ is the spectral density of turbulence in along-wind direction (Kaimal's longitudinal wind spectrum); ψ_{ni} is a random variable uniformly distributed between 0 and 2π ; $\Delta\omega = \omega_{up} / N_f$ = the frequency increment; ω_{up} is the upper cut-off frequency with the condition that the value of $S_w(\omega)$ is less than a pre-set small number ϵ when $\omega > \omega_{up}$; and the related wind spectrums used in Eq. (8) are given by

(1) Horizontal wind spectrum

$$S_H(\omega) = \frac{200 \times \bar{U}^2}{\left[1 + 50 \frac{\omega}{2\pi} \left(\frac{z}{V_0}\right)\right]^{5/3}} \left(\frac{z}{V_0}\right) \quad (9a)$$

(2) Lateral wind spectrum

$$S_L(\omega) = \frac{15 \times \bar{U}^2}{\left[1 + 9.5 \frac{\omega}{2\pi} \left(\frac{z}{V_0}\right)\right]^{5/3}} \left(\frac{z}{V_0}\right) \quad (9b)$$

(3) Vertical wind spectrum

$$S_V(\omega) = \frac{3.36 \times \bar{U}^2}{\left[1 + 10 \frac{\omega}{2\pi} \left(\frac{z}{V_0}\right)\right]^{5/3}} \left(\frac{z}{V_0}\right) \quad (9c)$$

with the steady wind speed of $\bar{U} = KV_0 / \ln(z/z_0)$ and

$$G_{jn}(\omega) = \begin{cases} 0 & 1 \leq j < n \leq N_s \\ C^{|j-n|} & n = 1, n \leq j \leq N_s \\ C^{|j-n|} \sqrt{1-C^2} & 2 \leq n \leq j \leq N_s \end{cases} \quad (10a)$$

$$C = \exp\left(\frac{-\lambda \omega \times \ell_{jn}}{2\pi V_0}\right) \quad (10b)$$

Here, V_0 = mean velocity of wind at height z , \bar{U} stands for the shear velocity of airflow related to von Karman's constant $K = 0.4$ and the ground roughness z_0 ; λ is an exponential decay factor taken between 7 and 10; ℓ_{jn} is the distance between the simulated points j and n ; and $C^{|j-n|}$ is the coherence function between points j and n (Xu et al. 2003). In this article, the following wind parameters are used: $z = 30\text{m}$, $z_0 = 0.012$ for open site, and $\lambda = 7$.

4 VBI finite element model

To deal with the present wind/VBI dynamic analysis for indirect bridge frequency measurement, the following assumptions are considered in modelling the vehicle-bridge system:

- (1) The 3D Bernoulli-Euler beam-column elements are used to model the bridge decks and towers of the cable-stayed bridge studied herein.
- (2) The road cars running on the bridge are assumed to travel at constant speed and the two-axle vehicle is considered (see Fig. 4).
- (3) The interactions of the vehicle-bridge system are regarded as no separation and side slipping of the wheels of running vehicles.
- (4) The vehicle accidents running on bridge deck, such as overturning and lateral sliding, would be excluded in the present investigations.

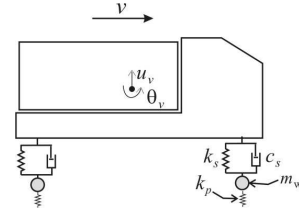


Fig. 4 Two-axle vehicle model

With the assumption (1) described above, as shown in Fig. 5(a), three major components of the cable-stayed bridge modelled by finite elements are described as follows: (1) The bridge deck is modelled as a number of beam-column elements incorporating all the axial and inertial properties. (2) Each of the towers is modelled by a number of beam-column elements with the axial and flexibility. (3) Each stay cable is represented as a two-node bar or truss element of which the axial stiffness is related to the axial tension. The curved cable is represented by a tensile bar element considering the sagging effect caused by self-weight, in which the equivalent modulus E_{eq} of the cable proposed by Ernst (1965) is given as

$$E_{eq} = \frac{E_s}{1 + \frac{(w_c L_h)^2 (T_i + T_f) E_s A_c}{24 (T_i T_f)^2}} \quad (11)$$

where E_s is the elastic modulus, L_h the horizontal projected length, w_c the weight per unit length, A_c the cross-sectional area, and T_i the initial cable tension resulting from the dead loads of the bridge and T_f the final cable tension caused by the real acting loads including vehicular loads and wind actions. The equation of motion of the whole bridge and vehicle under wind actions are written as

$$[m_b] \{\ddot{u}_b\} + [c_b] \{\dot{u}_b\} + [k_b] \{u_b\} = \{p_{b,w}\} - \{f_c\} \quad (12)$$

$$[m_c] \{\ddot{u}_c\} + [c_c] \{\dot{u}_c\} + [k_c] \{u_c\} = \{p_{c,w}\} + \{p_c\} + \{f_c\}$$

where $[m_b]$, $[c_b]$, $[k_b]$ denote the mass, damping, and stiffness matrices, $\{u_b\}$ the displacements of the beam element, $\{p_{b,w}\}$ nodal aerodynamic forces acting on the beam element, and $\{f_c\}$ the contact forces existing between the vehicle system and the beam element. Also, $[m_c]$, $[c_c]$, $[k_c]$ denote the mass, damping, and stiffness matrices of the sprung mass, $\{u_c\}$ the vertical deflections of the wheel and sprung masses, and $\{p_{c,w}\}$ aerodynamic forces acting on the moving vehicles. Here, the aerodynamic force vectors of $\{p_{b,w}\}$ and $\{p_{c,w}\}$ were described in detail in Section 2.

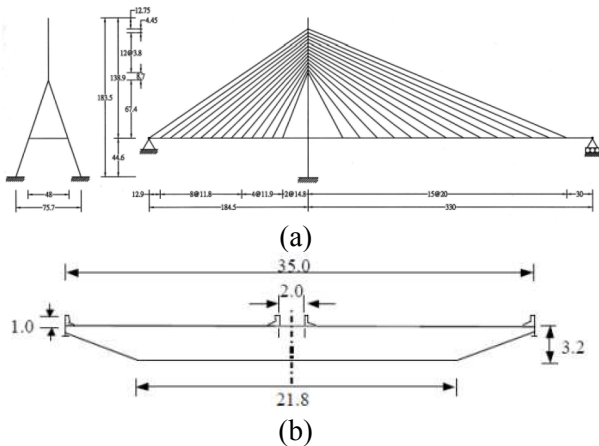


Fig. 5 Schematic diagram and cross section of the Kao-Pin-Hsi cable-stayed bridge

Following the nonlinear analysis procedure of the wind/VBI system based on the incremental-iterative approach (Yau and Kuo 2014), the numerical demonstration will be presented in the following.

5 Numerical Illustrations

Figure 5 shows a schematic diagram of KPH cable-stayed bridge for highway in southern Taiwan. The bridge deck is supported by a roller on the horizontal beams of the “A” pylons. The pylon is made of concrete with elastic modulus $E_c = 35\text{GPa}$ and density $\rho_c = 2.4\text{t/m}^3$, and the steel bridge deck and stay cable with $E_s = 210\text{GPa}$ and $\rho_s = 7.8\text{t/m}^3$. Rayleigh damping is assumed for the bridge with a damping ratio of 2%. The sectional properties of the cable-stayed bridge are given as follow: (1) cross-sectional area of the left/right bridge deck $A_b = 21.6 / 1.74\text{m}^2$, (2) cross-sectional area of the pylon $A_p = 42\text{m}^2$, (3) moment of inertia of the left / right bridge deck $I_{bY} = 132.60 / 16 \text{ m}^4$, $I_{bZ} = 2122 / 90 \text{ m}^4$, $J = 31.3 / 3 \text{ m}^4$. By free vibration analysis and field measurements, the natural frequencies of the bridge in three directions are shown below:

Table 1 Comparison of KPH bridge frequencies

Vibration mode	Frequency (Hz) (FE analysis)	Frequency (Hz) (field measurement)
Vertical	0.28, 0.54	0.28, 0.57
Lateral	0.67, 1.15	0.64
Torsional	0.74, 1.53	0.75

Here, the measured frequencies are compared with the present results. For illustration, let us consider stationary traffic flow with a raw of identical moving road cars, in which the axle-interval of 6m. According to empirical formula proposed by the

Ministry of Transportation in Taiwan, the safety interval between two moving cars at the same lane of highway is estimated as $v-20$ (m), in which the moving speed v is represented by km/h. Let the moving speed be 72km/h and the following car data are used considering traffic flow: (1) mass of the road cars $M_v = 5\text{t}$, (2) pitching moment of inertia $I_v = 15\text{m}^4$, (3) suspension unit: $k_s = 480\text{kN/m}$, $c_s = 8.5 \text{ kN-s/m}$. And the following data are used for the test vehicle: (1) $M_v = 1.5\text{t}$, $I_v = 2\text{m}^4$, $k_s = 180\text{kN/m}$, $c_s = 4.5\text{kN-s/m}$.

The time history responses of vertical and lateral acceleration of the running test vehicle have been plotted in the Figs. 6 and 7, respectively. With the predicted aerodynamic coefficients and the traffic flow, one can carry out the time-history analysis of interaction dynamic response of wind/VBI system for the KPH bridge. As indicated in Fig. 6, the vertical acceleration response of the test vehicle is rather irregular due to pavement roughness of roadway. On the other hand, the lateral acceleration response, as shown in Fig. 7, a periodic peaks exist on the response curve due to lateral wind-induced vibration of the bridge deck, which is a detecting benefit for us to identify the lateral frequencies of the cable-stayed bridge.

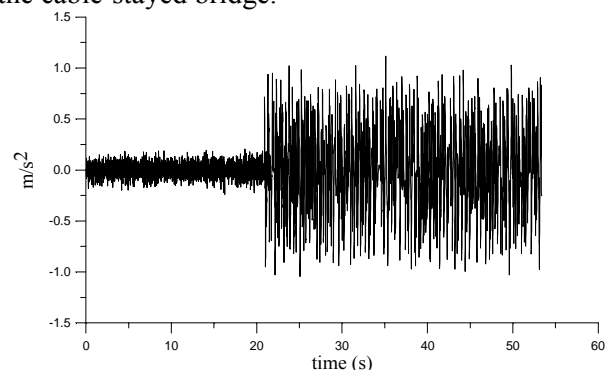


Fig. 6 Time history response of vertical acceleration of the test vehicle

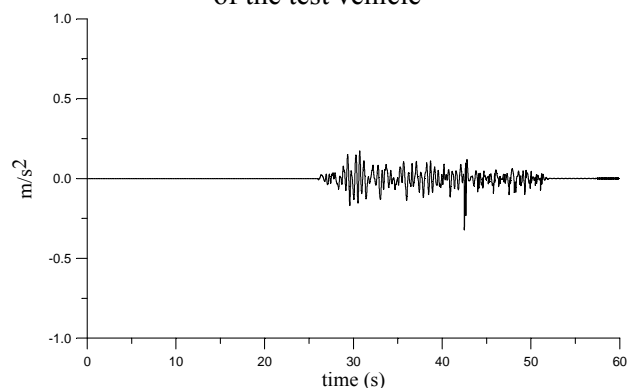


Fig. 7 Time history response of lateral acceleration of the instrumented car

Based on the indirect measurement approach proposed by Yang et al. (2004), the normalized FFT responses in frequency domain of both the vertical and lateral acceleration response of the running vehicle have been plotted in the following Fig. 8.

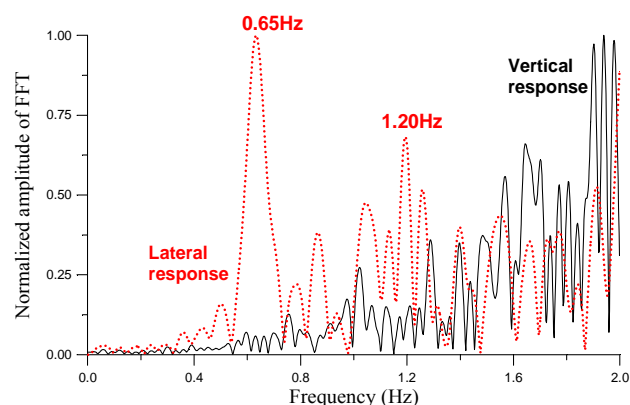


Fig. 8 FFT of lateral acceleration response of the test vehicle

As shown in Fig. 8, two significant peaks exist around 0.68Hz and 1.2Hz in the FFT-frequency plot for the lateral acceleration response of the test vehicle, which indicated that the first two lateral bridge frequencies were captured by the running test vehicle as the long-span cable-stayed bridge in cross winds. But the test vehicle fails to detect the flexural frequencies in vertical direction of the bridge, as shown in Fig. 8, due to the inference of pavement roughness.

6 Concluding remarks

In this study, an iteration-based wind/VBI FE analysis was carried out and used to detect the lateral frequency of a long-span cable-stayed bridge using a passing test vehicle. The numerical studies demonstrated that the present indirect method is feasible to identify the lateral bridge frequency as the test vehicle running on the bridge in cross winds. A further study on field measurements and wind tunnel tests needs to be investigated for experimental verifications.

Acknowledgement

This research was partially supported by the Ministry of Science and Technology in Taiwan through the Taiwan-Czech joint project with the Grants: MOST 103-2923-E-032-002-MY3, 105-2221-E-032-005, 106-2923-E-002-007-MY3, and GA CR 17-26353J.

References:

- [1] Baker C.J. (1986) A simplified analysis of various types of wind-induced road vehicle accidents, *J. Wind Eng. Ind. Aerodyn.*, 22, 69–85.
- [2] Cai, C.S., Chen, S.R. (2004). Framework of vehicle–bridge–wind dynamic analysis, *J. Wind Eng. and Ind. Aerodyn.* 92, 579–607.
- [3] Ernst, J.H. (1965), Der E-modul von seilen unter Berücksichtigung des durchhanges, *Bauingenieur* 40 (2) 52–55.
- [4] Simiu, E., Scanlan, R.H. (1996), *Wind Effects on Structures-Fundamentals and Applications to Design*, 3rd Ed., John Wiley & Sons, Inc., New York.
- [5] Xu, Y.L., Xia, H., Yan, Q.S. (2003), Dynamic response of long suspension bridge to high wind and running train. *ASCE J. Bridge Eng.* 8, 46–55.
- [6] Xu, Y.L., Zhang, N., Xia, H. (2004) Vibration of coupled train and cable-stayed bridge systems in cross winds, *Eng. Struct.* 26, 1389–1406.
- [7] Yang, Y.B., Lin, C.W., and Yau, J.D. (2004). Extracting bridge frequencies from the dynamic response of a passing vehicle, *J. Sound and Vib.*, 272(3-5): 471–493.
- [8] Yang, Y.B. and Lin, C.W. (2005). Vehicle-bridge interaction dynamics and potential applications, *J. Sound and Vib.*, 284(1-2): 205–226.
- [9] Yang, Y.B., and Chang, K.C. (2009). Extraction of bridge frequencies from the dynamic response of a passing vehicle enhanced by the EMD technique, *J. Sound and Vib.*, 322(4-5): 718–739.
- [10] Yang, Y.B., Li, Y.C., and Chang, K.C. (2012). Using two connected vehicles to measure the frequencies of bridges with rough surface: a theoretical study, *Acta Mech.*, 223(8): 1851–1861.
- [11] Yang, Y.B., Chang, K.C., and Li, Y.C. (2013a). Filtering techniques for extracting bridge frequencies from a test vehicle moving over the bridge, *Eng. Struct.*, 48: 353–362.
- [12] Yang, Y.B., Chen, W.F., Yu, H.W., and Chan, C.S. (2013b). Experimental study of a hand-drawn cart for measuring the bridge frequencies, *Eng. Struct.*, 57: 222–231.
- [13] Yang, Y.B., Cheng, M.C., and Chang, K.C. (2013c). Frequency variation in vehicle-bridge interaction systems, *Intl. J. Struct. Stab. Dyna.*, 13(2), 1350019.
- [14] Yang, Y.B., Li, Y.C., and Chang, K.C. (2014). Constructing the mode shapes of a bridge from a passing vehicle: a theoretical study, *Smart Struct. Syst.*, 13(5): 797–819.
- [15] Yau, J.D. and Kuo, S.R. (2014), Study on interaction aerodynamics of vehicle-bridge system under wind actions, 12th International Conference on Fluid Mechanics & Aerodynamics (FMA '14), Dec.29-31, Geneva, Switzerland.